Mecánica Computacional Vol. XXIII, pp. 3191-3209
G.Buscaglia, E.Dari, O.Zamonsky (Eds.)
Bariloche, Argentina, November 2004

A DOMAIN DECOMPOSITION PROCEDURE FOR THE SIMULATION OF WAVES IN FLUID SATURATED COMPOSITE POROVISCOELASTIC MEDIA

Claudia L. Ravazzoli†**and Juan E. Santos***

†Facultad de Ciencias Astronómicas y Geofísicas,
Universidad Nacional de La Plata, CONICET
Paseo del Bosque s/n, 1900 - La Plata, Argentina
e-mail: claudia@fcaglp.fcaglp.unlp.edu.ar

*Facultad de Ciencias Astronómicas y Geofísicas,
Universidad Nacional de La Plata, CONICET
Paseo del Bosque s/n, 1900 - La Plata, Argentina
e-mail: santos@fcaglp.fcaglp.unlp.edu.ar
Also Department of Mathematics, Purdue University,
W. Lafayette, IN, 47907, USA

Key Words: numerical simulation, poroviscoelasticity, wave propagation, composite solids.

Abstract. *This work presents an iterative domain decomposition finite element procedure to solve the equations describing wave propagation in a porous medium composed of two weakly coupled solids saturated by a single-phase fluid.*

The plane wave analysis for this model shows the existence of three compressional and two shear modes of propagation.

The equations of motion are formulated in the space-frequency domain including dissipation in the solid matrix and frequency correction factors in the mass and viscous coupling coefficients. First order absorbing boundary conditions are employed at the artificial boundaries of the computational domain.

Examples showing the application of the algorithm for the numerical simulation of ultrasonic wave propagation in a sample of water saturated partially frozen Berea sandstone are presented and analyzed.

1 INTRODUCTION

Wave propagation in composite porous materials has applications in many branches of science and technology, such as seismic methods in the presence of shaley sandstones,[1] frozen or partially frozen sandstones,[2–4] gas-hydrates in ocean-bottom sediments[5] and evaluation of the freezing conditions of foods by ultrasonic techniques.[6]

Both frozen porous media and shaley sandstones are two examples of porous materials where the two solid phases are *weakly-coupled* or *non-welded*, i.e, both solids form a continuous and interacting composite structure, interchanging mechanical energy.

This article presents a differential and numerical model to describe wave propagation in a heterogeneous poroviscolastic frame consisting of two weakly-coupled solid phases saturated by a single phase fluid. The model, stated in the space-frequency domain, generalizes that presented in[7] by the inclusion of solid matrix dissipation using a linear viscoelastic model and frequency dependent mass and viscous coupling coefficients.

Numerical simulation of waves in porous media is computationally expensive due to the large number of degrees of freedom needed to calculate wave fields accurately; the use of a domain decomposition iteration is a convenient approach to overcome this difficulty. The type of domain decomposition procedure used in this paper was presented in[8] for solving second-order elliptic problems. The algorithm employs the nonconforming rectangular element defined in[9] to approximate the displacement vector in the solid phases. The displacement in the fluid phase is approximated by using the vector part of the Raviart-Thomas-Nedelec mixed finite element space of zero order, which is a conforming space.[10,11]

This numerical procedure is used for the simulation of waves in a sample of water saturated partially frozen Berea sandstone,[5,12] perturbed by a point source at ultrasonic frequencies. We show snapshots of the generated wavefields, where the events associated with the different types of waves can be clearly observed.

2 THE DIFFERENTIAL MODEL

Here we review and generalize a model recently presented by the authors,[12],[7] to describe the propagation of waves in a poroelastic domain consisting of a matrix of two different solids indicated by the indices or supraindices 1 and 3, saturated by a single phase fluid indicated by the index or supraindex 2. Thus, for any elementary cube Q of bulk material we have

$$Q = Q_1 \cup Q_2 \cup Q_3.$$

Let V_i denote the volume of the phase Q_i and let us denote by V_b and V_{sm} the bulk volume of Q and the solid matrix $Q_{sm} = Q_1 \cup Q_3$, respectively so that

$$V_{sm} = V_1 + V_3, \qquad V_b = V_1 + V_2 + V_3$$

We introduce the bulk volumetric fractions of the different components in the form:

$$\phi = \frac{V_2}{V_b}, \quad \phi_1 = \frac{V_1}{V_b}, \quad \phi_3 = \frac{V_3}{V_b}, \tag{1}$$

and we also introduce the solid fractions of the composite matrix

$$S_1 = \frac{V_1}{V_{sm}}, \;\; S_3 = \frac{V_3}{V_{sm}}, \;\; \text{with} \;\; S_1 + S_3 = 1. \tag{2}$$

For some practical applications it is convenient to define the *absolute* or *effective porosity* of the medium, defined as the ratio of the volume of the interconnected pores V_p and the total volume of the sample, i.e,

$$\phi_a = \frac{V_p}{V_b}. \tag{3}$$

These set of fractions can have different meanings depending on the physical model considered. For example, in the case of a sandstone or soil at very low temperature, it is reasonable to consider that a part of the fluid which saturates the pore space is at a liquid state and the rest is frozen. If Q_1 represents the mineral grains and Q_3 the ice, for a given porosity ϕ_a and *bulk water content* ϕ the following relations can be found:

$$\phi_1 = 1 - \phi_a, \tag{4}$$

$$\phi_3 = \phi_a - \phi, \tag{5}$$

$$S_3 = \frac{\phi_3}{1 - \phi}. \tag{6}$$

It is useful to introduce an additional fraction S_3' to account for the *ice content in the pores*, given by

$$S_3' = \frac{V_3}{V_p} = \frac{\phi_3}{1 - \phi_1}. \tag{7}$$

A different application of this model would be the case of a shaley sandstone, that is, a porous rock mainly composed of quartz grains and clay particles, saturated by a fluid (such as water, brine, gas or oil). In this case we assume that the fluid completely saturates the pore space of the composite rock so that $V_2 \equiv V_p$. Then, if Q_1 represents the grains of the rock and Q_3 the clay part, for a given *matrix clay content* S_3 and water content ϕ we have:

$$\phi = \phi_a, \tag{8}$$

$$\phi_1 = S_1(1 - \phi), \tag{9}$$

$$\phi_3 = S_3(1 - \phi). \tag{10}$$

Now let us consider a poroelastic bounded domain $\Omega = \Omega_1 \cup \Omega_2 \cup \Omega_3$. Since by hypothesis the two solids are non-welded (or weakly coupled), we assume that they can move independently

and consequently we can distinguish three different particle displacement fields for this model. Let $u^{(1)},\ u^{(2)}$ and $u^{(3)}$ be the averaged absolute solid and fluid displacements over the bulk material Ω. Also, let the relative flow of the fluid phase with respect to the composite solid matrix be defined by

$$w = \phi(u^{(2)} - S_1 u^{(1)} - S_3 u^{(3)}), \tag{11}$$

and set $u = (u_1, w, u_3)$. As explained in[7] the variable

$$\zeta = -\nabla \cdot w \tag{12}$$

represents the change in fluid content.

Next we introduce the local stress tensors $\sigma_{ij}^{(1)}$ and $\sigma_{ij}^{(3)}$ in Ω_1 and Ω_3, averaged over the bulk material and the fluid pressure p_f. Following[7] we define the second order tensors

$$\sigma^{(1,T)} = \sigma_{ij}^{(1)} - S_1\phi p_f \delta_{ij}, \qquad \sigma^{(3,T)} = \sigma_{ij}^{(3)} - S_3\phi p_f \delta_{ij}, \tag{13}$$

associated with the total stresses in Ω_1 and Ω_3, respectively. Let $\widehat{f}(\omega)$ denote the time-Fourier transform of $f(t)$, with ω being the angular frequency. Then the constitutive equations, stated in the space-frequency domain are[7]

$$\widehat{\sigma}_{ij}^{(1,T)}(\widehat{u}) = \left[\lambda_1\widehat{\theta}_1 - B_1\widehat{\zeta} + B_3\widehat{\theta}_3\right]\delta_{ij} + 2\mu_1\widehat{\epsilon}_{ij}^{(1)} + \mu_{1,3}\widehat{\epsilon}_{ij}^{(3)}), \tag{14}$$

$$\widehat{\sigma}_{ij}^{(3,T)}(\widehat{u}) = \left[\lambda_3\widehat{\theta}_3 - B_2\widehat{\zeta} + B_3\widehat{\theta}_1\right]\delta_{ij} + 2\mu_3\widehat{\epsilon}_{ij}^{(3)} + \mu_{1,3}\widehat{\epsilon}_{ij}^{(1)}, \tag{15}$$

$$\widehat{p}_f(\widehat{u}) = -B_1\widehat{\theta}_1 - B_2\widehat{\theta}_3 + K_{av}\widehat{\zeta}. \tag{16}$$

where $\widehat{\epsilon}_{ij}^{(m)} = \epsilon_{ij}(\widehat{u}^{(m)})$ being the Fourier transform of the strain tensor with linear invariant $\widehat{\theta}_m$.

The coefficients in (14)-(16) may be complex and frequency dependent. They can be determined in terms of the properties of the individual solid and fluid phases as explained in the Appendix.

Let the positive definite mass matrix $\mathcal{P} = \mathcal{P}(\omega) \in \mathbf{R}^{9\times 9}$ and the nonnegative dissipation matrix $\mathcal{B} = \mathcal{B}(\omega) \in \mathbf{R}^{9\times 9}$ be defined by

$$\mathcal{P} = \begin{bmatrix} p_{11}I & p_{12}I & p_{13}I \\ p_{12}I & p_{22}I & p_{23}I \\ p_{13}I & p_{23}I & p_{33}I \end{bmatrix}, \qquad \mathcal{B} = \begin{bmatrix} b_{11}I & -b_{12}I & -b_{11}I \\ -b_{12}I & b_{22}I & b_{12}I \\ -b_{11}I & b_{12}I & b_{11}I \end{bmatrix}$$

where I denotes the identity matrix in $\mathbf{R}^{3\times 3}$. The coefficients $p_{ij} = p_{ij}(\omega), b_{ij} = b_{ij(\omega)}$ in the definition of the matrices $\mathcal{P}$ and $\mathcal{B}$ can be computed as explained in the Appendix.

Also, let $\mathcal{L}(\widehat{u})$ be the second order differential operator defined by

$$\mathcal{L}(\widehat{u}) = \left\{ \nabla \cdot \widehat{\sigma}_{ij}^{(1,T)}(\widehat{u}), -\nabla \widehat{p}_f(\widehat{u}), \nabla \cdot \widehat{\sigma}_{ij}^{(3,T)}(\widehat{u}) \right\}.$$

Then the equations of motion in Ω are[7]

$$-\omega^2 \mathcal{P}\widehat{u} + i\omega \mathcal{B}\widehat{u} - \mathcal{L}(\widehat{u}) = \widehat{S}(x,\omega), \quad (x,\omega) \in \Omega \times (0,\omega^*), \tag{17}$$

where $S(x,\omega) = (S^1(x,\omega), S^f(x,\omega), S^3(x,\omega)$ denotes the external source and ω^* is an upper temporal frequency of interest.

A plane wave analysis shows that three different compressional waves (P1, P2 and P3) and two shear waves (S1, S2) can propagate,[13].[7] The P1 and S1 waves correspond to the classical fast P and S waves propagating in elastic or viscoelastic isotropic solids. The additional slow modes are waves strongly attenuated in the low frequency range, related to motions out of phase of the different phases. The experimental observation of the additional (slow) waves was reported by Leclaire et al.[14]

The slow wave modes are important to explain attenuation and dispersion effects observed on the faster modes associated with scattering phenomena due to the presence of heterogeneities inside the composite poroelastic medium.

3 THE DOMAIN DECOMPOSITION ITERATION

We consider the solution of (17) in a rectangular poroviscoelastic domain Ω in the (x,z)–plane using a domain decomposition procedure. Let $\mathcal{N}^h$ be a nonoverlapping partition of Ω into rectangles Ω_j of diameter bounded by h such that $\overline{\Omega} = \cup_{j=1}^{J} \overline{\Omega}_j$. Set $\Gamma_j = \partial\Omega \cap \partial\Omega_j$, $\Gamma_{jk} = \partial\Omega_j \cap \partial\Omega_k$, and denote by ξ_j and ξ_{jk} the midpoints of Γ_j and Γ_{jk}, respectively. Let us denote by ν_{jk} the unit outer normal on Γ_{jk} from Ω_j to Ω_k and by ν_j the unit outer normal to Γ_j. Let χ_j and χ_{jk} be two unit tangents on Γ_j and Γ_{jk} so that $\{\nu_j, \chi_j\}$ and $\{\nu_{jk}, \chi_{jk}\}$ are orthonormal systems on Γ_j and Γ_{jk}, respectively. Set

$$\begin{aligned}
\mathcal{G}_j(\widehat{u}_j) = \Big(& \widehat{\sigma}^{(1,T)}(\widehat{u}_j)\nu_j \cdot \nu_j, \widehat{\sigma}^{(1,T)}(\widehat{u}_j)\nu_j \cdot \chi_j, \widehat{p}_f(\widehat{u}_j), \\
& \widehat{\sigma}^{(3,T)}(\widehat{u}_j)\nu_j \cdot \nu_j, \widehat{\sigma}^{(3,T)}(\widehat{u}_j)\nu_j \cdot \chi_j \Big), \qquad (x,z) \in \Gamma_j, \\
\mathcal{G}_{jk}(\widehat{u}_j) = \Big(& \widehat{\sigma}^{(1,T)}(\widehat{u}_j)\nu_{jk} \cdot \nu_{jk}, \widehat{\sigma}^{(1,T)}(\widehat{u}_j)\nu_{jk} \cdot \chi_{jk}, \widehat{p}_f(\widehat{u}_j), \\
& \widehat{\sigma}^{(3,T)}(\widehat{u}_j)\nu_{jk} \cdot \nu_{jk}, \widehat{\sigma}^{(3,T)}(\widehat{u}_j)\nu_{jk} \cdot \chi_{jk} \Big), \quad (x,z) \in \Gamma_{jk}, \\
\Pi_{\Gamma_j}(u_j) = & \left(u_j^1 \cdot \nu_j, u_j^1 \cdot \chi_j, w_j \cdot \nu_j, u_j^3 \cdot \nu_j, u_j^3 \cdot \chi_j \right), \qquad (x,z) \in \Gamma_j, \\
\Pi_{\Gamma_{jk}}(u_j) = & \left(u_j^1 \cdot \nu_{jk}, u_j^1 \cdot \chi_{jk}, w_j \cdot \nu_{jk}, u_j^3 \cdot \nu_{jk}, u_j^3 \cdot \chi_{jk} \right), \qquad (x,z) \in \Gamma_{jk}.
\end{aligned}$$

If Ω_j has a part Γ_j of its boundary contained in $\partial\Omega$, we impose the absorbing boundary condition (see[15])

$$-\mathcal{G}_j(u_j) = i\omega\mathcal{A}\Pi_{\Gamma_j}(u_j), \qquad (x,z) \in \Gamma_j, \tag{18}$$

where the symmetric positive definite matrix $\mathcal{A}$ is given by[15] $\mathcal{A} = \mathcal{M}^{\frac{1}{2}}\mathcal{D}^{\frac{1}{2}}\mathcal{M}^{\frac{1}{2}}$ with $\mathcal{D} = \mathcal{M}^{-\frac{1}{2}}\mathcal{E}\mathcal{M}^{-\frac{1}{2}}$ and

$$\mathcal{M} = \begin{bmatrix} m_{11} & 0 & m_{12} & m_{13} & 0 \\ 0 & q_1 & 0 & 0 & q_2 \\ m_{12} & 0 & m_{22} & m_{33} & 0 \\ m_{13} & 0 & m_{23} & m_{33} & 0 \\ 0 & q_2 & 0 & 0 & q_3 \end{bmatrix}, \qquad \mathcal{E} = \begin{bmatrix} \lambda_1+2\mu_1 & 0 & B_1 & B_3+\frac{1}{2}\mu_{13} & 0 \\ 0 & \mu_1 & 0 & 0 & \frac{1}{2}\mu_{13} \\ B_1 & 0 & M & B_2 & 0 \\ B_3+\frac{1}{2}\mu_{13} & 0 & B_2 & \lambda_3+2\mu_3 & 0 \\ 0 & \frac{1}{2}\mu_{13} & 0 & 0 & \mu_3 \end{bmatrix},$$

Furthermore, as in[16,17] at the interior interface Γ_{jk} we use the Robin transmission boundary conditions:

$$\mathcal{G}_{jk}(u_j) + i\omega\beta_{jk}\Pi_{\Gamma_{jk}}(u_j) = \mathcal{G}_{kj}(u_k) - i\omega\beta_{jk}\Pi_{\Gamma_{kj}}(u_k), \quad (x,z) \in \Gamma_{jk} \subset \partial\Omega_j, \tag{19}$$
$$\mathcal{G}_{kj}(u_k) + i\omega\beta_{jk}\Pi_{\Gamma_{kj}}(u_k) = \mathcal{G}_{jk}(u_j) - i\omega\beta_{jk}\Pi_{\Gamma_{jk}}(u_j), \quad (x,z) \in \Gamma_{jk} \subset \partial\Omega_k. \tag{20}$$

Here β_{jk} is a positive definite matrix function defined on the interior boundaries Γ_{jk}. The Robin transmission conditions (19)–(20) impose the continuity of the solid displacement, the normal component of the fluid displacements and the generalized stresses at the interior interfaces Γ_{jk}. The spatial discretization is performed as follows. To approximate each component of the solid displacement vector we employ the nonconforming finite element space as in,[9] while to approximate the fluid displacement vectors we choose the vector part of the Raviart-Thomas-Nedelec space[10,11] of zero order. More specifically, set

$$\widehat{R} = [-1,1]^2, \qquad \widehat{\mathcal{V}}(\widehat{R}) = \text{Span}\{1, \hat{x}, \hat{y}, \theta(\hat{x}) - \theta(\hat{z})\}, \quad \theta(\hat{x}) = \hat{x}^2 - \frac{5}{3}\hat{x}^4.$$

with the degrees of freedom being the values at the midpoint of each edge of $\widehat{R}$. Also, if $\psi^L(\hat{x}) = -1 + \hat{x}$, $\psi^R(\hat{x}) = \hat{x}$, $\psi^B(\hat{z}) = -1 + \hat{z}$, $\psi^T(\hat{z}) = \hat{z}$, we have that

$$\widehat{\mathcal{W}}(\widehat{R}) = \text{Span}\big\{(\psi^L(\hat{x}),0), (\psi^R(\hat{x}),0), (0,\psi^B(\hat{z})), (0,\psi^T(\hat{z}))\big\}.$$

For each Ω_j, let $F_{\Omega_j} : \widehat{R} \to \Omega_j$ be an invertible affine mapping such that $F_{\Omega_j}(\widehat{R}) = \Omega_j$, and define

$$\mathcal{V}_j^h = \{v = (v_1, v_2) : \ v_i = \widehat{v}_i \circ F_{\Omega_j}^{-1}, \ \widehat{v}_i \in \widehat{\mathcal{V}}(\widehat{R}), \ i = 1,2\},$$
$$\mathcal{W}_j^h = \{w : \ w = \widehat{w} \circ F_{\Omega_j}^{-1}, \ \widehat{w} \in \widehat{\mathcal{W}}(\widehat{R})\}.$$

Next, following,[9,16,17] we introduce a set of Lagrange multipliers $\eta_{jk} = (\eta_{jk}^{1,\nu}, \eta_{jk}^{1,\chi}, -\eta_{jk}^{f}, \eta_{jk}^{3,\nu}, \eta_{jk}^{3,\chi})$ associated with the values of the generalized forces at the mid points ξ_{jk} of Γ_{jk} in the sense that $\eta_{jk} \sim \mathcal{G}_{jk}(U_j)(\xi_{jk})$. The Lagrange multipliers η_{jk} belong to the following space of functions defined on the interior interfaces Γ_{jk}:

$$\Lambda^h = \big\{\eta\colon \eta|_{\Gamma_{jk}} = \eta_{jk} \in [P_0(\Gamma_{jk})]^5 = \Lambda_{jk}^h,\ \forall\{j,k\}\big\},$$

where $P_0(\Gamma_{jk})$ denotes the constant functions on Γ_{jk}.

Next, we state a domain decomposition iteration using a variational formulation. Let us denote by $(\cdot,\cdot)_j$ the usual complex inner product in $L^2(\Omega_j)$. Moreover, for $\Gamma = \Gamma_j$ or $\Gamma = \Gamma_{jk}$ let $\langle\cdot,\cdot\rangle_\Gamma$ denote the complex inner product in $L^2(\Gamma)$, and let $\langle\langle u, v\rangle\rangle_\Gamma$ denote its approximation by the mid–point quadrature: $\langle\langle u, v\rangle\rangle_\Gamma = (u\overline{v})(\xi_{jk})|\Gamma|$ where $|\Gamma|$ is the measure of Γ. Then the domain decomposition iteration is defined as follows: given $(U_j^0, \eta_{jk}^0) \in \mathcal{V}_j^h \times \mathcal{W}_j^h \times \mathcal{V}_j^h \times \Lambda_{jk}^h$ for all j, for $t = 1, 2, 3, \cdots$, find $(U_j^t, \eta_{jk}^t) \in \mathcal{V}_j^h \times \mathcal{W}_j^h \times \mathcal{V}_j^h \times \Lambda_{jk}^h$ such that

$$\begin{aligned}
&-\omega^2\left(\mathcal{P}\,U_j^t,\ v\right)_j + i\omega\left(\mathcal{C}\,U_j^t,\ v\right)_j + \sum_{pq}\left(\widehat{\sigma}_{pq}^{(1,T)}(U_j^t),\ \varepsilon_{pq}(v^1)\right)_j \\
&-\left(\widehat{p}_f(U_j^t),\ \nabla\cdot v^2\right)_j + \sum_{pq}\left(\widehat{\sigma}_{pq}^{(3,T)}(U_j^t),\ \varepsilon_{pq}(v^3)\right)_j \qquad (21)\\
&+\left\langle\left\langle i\,\omega\mathcal{B}\Pi_{\Gamma_j}(U_j),\ \Pi_{\Gamma_j}(v)\right\rangle\right\rangle_{\Gamma_j} + \sum_k\left\langle\left\langle i\,\omega\beta_{jk}\Pi_{\Gamma_{jk}}(U_j), \Pi_{\Gamma_{jk}}(v)\right\rangle\right\rangle_{\Gamma_{jk}} \\
&= \left(S^1,\ v^1\right)_j + \left(S^f,\ v^2\right)_j + \left(S^3,\ v^3\right)_j \\
&\quad -\sum_k\left\langle\left\langle i\,\omega\beta_{jk}\Pi_{\Gamma_{kj}}(U_k^{t-1}),\ \Pi_{\Gamma_{jk}}(v)\right\rangle\right\rangle_{\Gamma_{jk}} - \sum_k\left\langle\left\langle(-\eta_{kj}^{t-1}, \Pi_{\Gamma_{jk}}(v)\right\rangle\right\rangle_{\Gamma_{jk}}, \\
&\qquad\qquad v = (v^1, v^2, v^3) \in \mathcal{V}_j^h \times \mathcal{W}_j^h \times \mathcal{V}_j^h \times \Lambda_{jk}^h, \\
&\eta_{jk}^{\nu,t} = \eta_{kj}^{\nu,t-1} - i\omega\beta_{jk}\left(\Pi_{\Gamma_{jk}}(U_j^t) + \Pi_{\Gamma_{kj}}(U_k^{t-1})\right)(\xi_{jk}). \qquad (22)
\end{aligned}$$

Equation (22), used to update the Lagrange multipliers, is obtained directly from (19) evaluated at the mid point ξ_{jk}. Equation (21) yields a 20×20 linear system of equations for the degrees of freedom associated with the vector displacements of the three phases on each subdomain Ω_j at the $t-$iteration level. The iteration (21)–(22) is a Jacobi–type iteration. A twice as fast iteration may also be defined by using a **red–black** type iteration (see[16,17]).

The choice of the nonconforming element used to compute the solid displacement is based on the dispersion analysis performed in[18] showing that it almost halves the number of points per wavelength needed to reach a desired accuracy as compared with the standard conforming bilinear element. The iteration parameter matrix β_{jk} is chosen to have the same form of the

matrix $\mathcal{A}$ in (18). The space–time solution is obtained by solving (21)–(22) for a finite number of frequencies and using an approximate inverse Fourier transform.[19] The definition of the iteration (21)–(22) can be extended to the case of larger subdomains Ω_j, see.[20]

4 NUMERICAL EXPERIMENTS

We consider wave propagation in a sample of water saturated partially frozen Berea sandstone, with an interior plane interface Γ defined by a change in ice content in the pores. The material properties of the system, taken from Refs.[5,12] are given in Table 1. In this case Ω_1 and Ω_3 correspond to the sandstone and ice, respectively. The computational domain Ω is a square of side length $L = 3$ cm with a uniform partition of Ω into squares of side length $h = L/N_x$, with $N_x = N_z = 261$.

The source function (S^1, S^f, S^3) is a compressional and shear point source located at (x_s, z_s) = (1.5 cm, 1.0 cm) applied to the solid and fluid phases, with a band limited spectrum of central frequency equal to 500 kHz.

The absolute porosity of the sandstone is $\phi_a = .3$, with the bulk water content ϕ chosen such that the ice content S_3' in the pores changes from 66 percent in the upper layer to 33 percent in the lower layer. For variable temperatures, the bulk water content ϕ may be computed as function of temperature using the expressions given in Refs.[13] and.[5]

For the calculation of the elastic coefficients we need values for the bulk and shear modulus of the two solid (dry) frames, denoted by $K_{s1,m}, K_{s3,m}, \ \mu_{s1,m}$ and $\mu_{s3,m}$, respectively (see the Appendix). Following Refs.[5,13] and[7] it is assumed that $K_{s1,m}$= 14.4 GPa and that the modulus $\mu_{s1,m}, \ \mu_{s3,m}$ and $K_{s3,m}$ can be computed using a percolation-type model using the relations

$$\mu_{sj,m} = \big[\mu_{sj,m}^{(max)} - \mu_{sj,m}^{0}\big]\big[\frac{\phi_3}{1-\phi_1}\big]^{3.8} + \mu_{sj,m}^{0}, \quad j = 1, 3, \tag{23}$$

$$K_{s3,m} = \big[K_{s3,m}^{(max)} - K_{s3,m}^{0}\big]\big[\frac{\phi_3}{1-\phi_1}\big]^{3.8} + K_{s3,m}^{0},$$

where $\mu_{s1,m}^{(max)}, \mu_{s3,m}^{(max)}$ and $K_{s3,m}^{(max)}$ are computed using the Kuster and Toksöz's model,[21] taking the known values of $K_{s1}, \mu_{s1}, K_{s3}, \mu_{s3}$ for the background medium with inclusions of air, with properties K_a, μ_a (see Table 1). The moduli $\mu_{s1,m}^0, \ \mu_{s3,m}^0$ and $K_{s3,m}^0$ are appropriate reference values. Here we take

$$\mu_{s1,m}^0 = 13.3 \text{ GPa}, \ \ K_{s3,m}^0 = \mu_{s3,m}^0 = 0. \tag{24}$$

The viscoelastic parameters describing the dissipative behaviour of the saturated sandstone are (see the Appendix) $T_{1,M} = (2\pi 10)^{-1}$ms, $T_{2,M} = (2\pi 10^9)^{-1}$ms, for $M = K_{G1}, K_{G3}, \mu_1, \mu_3, \mu_{13}, D_3$. For the mean quality factors we take $\widehat{Q}_{K_{G1}} = \widehat{Q}_{K_{G3}} = \widehat{Q}_{\mu_1} = \widehat{Q}_{\mu_3}$ = 100 and $\widehat{Q}_{\mu_{13}} = \widehat{Q}_{D_3}$ = 200. The value of the Kozeny-Carman constant was taken to be 5.[22]

Solid grain	bulk modulus, K_{s1}	38.7 GPa
	shear modulus, μ_{s1}	39.6 GPa
	density, ρ_1	2650 kg/m^3
	permeability $\kappa_{1,0}$	1.07 10^{-13} m^2
Ice	bulk modulus, K_{s3}	8.58 GPa
	shear modulus, μ_{s3}	3.32 GPa
	density, ρ_3	920 kg/m^3
	permeability $\kappa_{3,0}$	5 10^{-4} m^2
Fluid	bulk modulus, K_f	2.25 GPa
	density, ρ_2	1000 kg/m^3
	viscosity, η	1.798 cP
Air	bulk modulus, K_a	1.5 10^{-4} GPa
	shear modulus, μ_a	0 GPa

Table 1. Material properties of the frozen sandstone model

Table 2 displays values of the phase velocity and attenuation factors at 500 kHz for the five different types of waves for the two–layer model used in this experiment.

	Ice content 0.66		Ice content 0.33	
Wave	phase velocity (Km/s)	attenuation (dB)	phase velocity (Km/s)	attenuation (dB)
Fast P1 wave	4.08	0.35	3.90	0.47
Slow P2 wave	1.37	5.20	1.05	7.88
Slow P3 wave	0.22	30.0	0.22	6.70
Fast S1 wave	2.72	0.58	2.58	0.74
Slow S2 wave	0.57	2.45	0.22	1.04

Table 2. Wave speeds and attenuation factors for all waves at frequency 500 kHz.

The following figures present snapshots of the wavefields for this experiment, generated after solving (21)–(22) for 110 equally spaced temporal frequencies in the interval $(0, 1\,\text{mHz})$. To understand and identify more clearly the various kinds of waves propagating in the computational domain we also computed the corresponding curl and divergence of the different snapshots, which are not inluded by brevity.

Figures 1a), 1b) and 1c) show respectively snapshots of the vertical component of the particle velocity of the three phases at $t = 0.005$ ms where we can observe that after arriving at the interface Γ, the direct P1 and P2 waves (P1D, P2D waves) have generated reflected and transmitted fast and slow shear and compressional waves. The strong wavefront at the bottom of the figure corresponds to the reflected P1 wave (P11R) generated after the P1D wave hits Γ.

There is also a transmitted P1 wave (P11T) at the top of the snapshots that is not seen because of its low amplitude. The other strong wavefront above Γ corresponds to the transmitted P1 wave (P12T) generated after the P2D wave arrives at Γ at approximately $t = 0.0035$ ms. The P2D wave also generated the reflected S1 wave (S12R) which wavefront is located approximately at $.5$ cm below Γ.

The snapshots of the vertical component of the particle velocity of the three phases at $t = 0.01$ ms shown in Figures 2a), 2b) and 2c) present even more complicated wave patterns. Here we describe some of them. The almost circular wavefront below the interface Γ corresponds to the slow S2 direct wave (S2D). The direct P2D wave arriving at Γ at $t = 0.0035$ ms has generated the reflected and transmitted P3 waves P32R and P32T seen below and above Γ, respectively, the reflected P2 wavefront (P22R) seen at the very bottom of the snapshots and the transmitted S1 wave (S12T) at the very top of the snapshots.

Finally, Figures 3a) and 3b) show snapshots of the particle velocity of the solid phases 1 and 3 at time $t = 0.02$ ms, respectively. The direct S2D wave seen as a partial circular wavefront and incident at Γ at $t = 0.0086$ ms has generated the transmitted and reflected P2 waves P22T and P22R at the top and bottom of the snapshots. Also, after hitting Γ, the S2D wave has generated the reflected and transmitted S2 waves S22R and S22T seen below and above Γ.

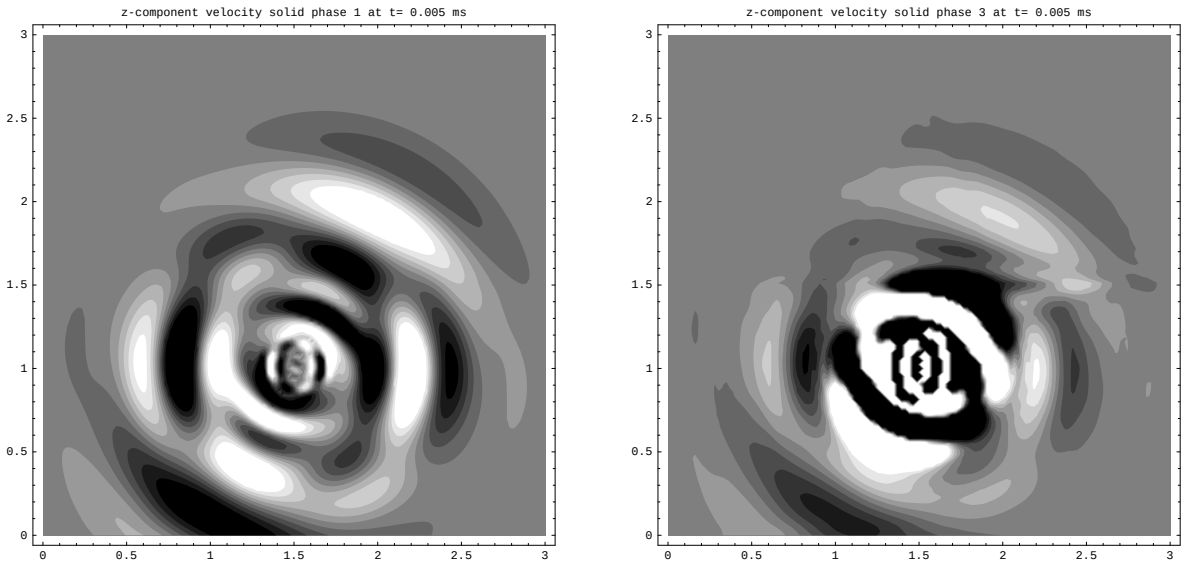

a) b)

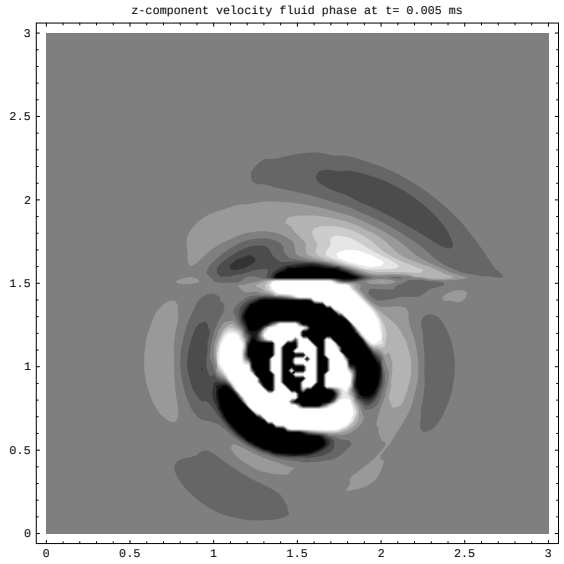

c)

Figure 1: Snapshots of the vertical particle velocity at $t = 0.005$ ms. The snapshots correspond to the solid phase 1 (a), the solid phase 3 (b) and the fluid phase (c). The relative amplitude relation between the snapshots in Figures 1a), 1b) and 1c) is $1/197/4$, respectively.

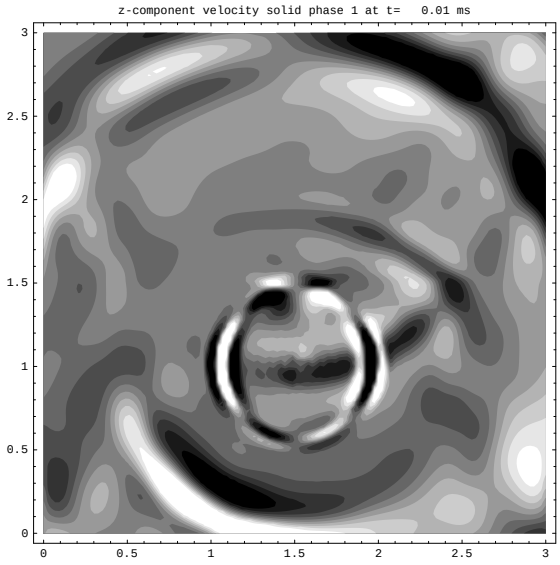

a)

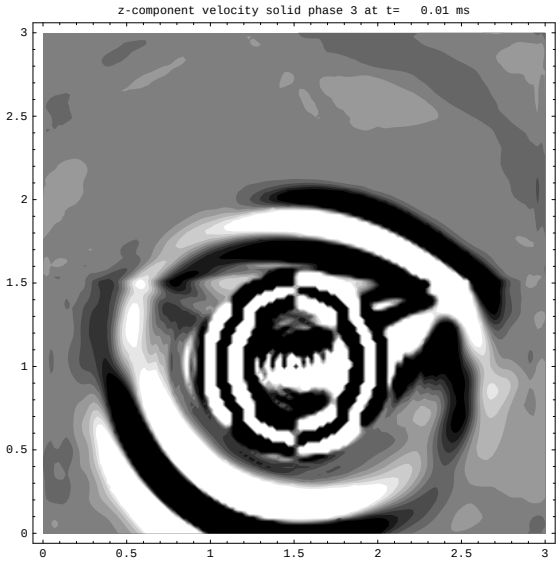

b)

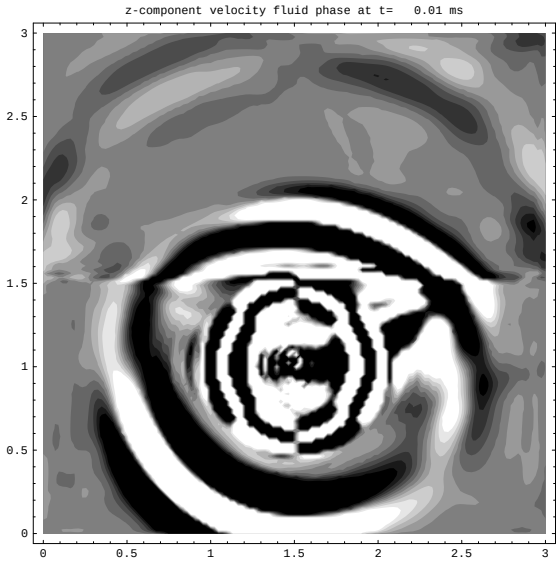

c)

Figure 2: Snapshots of the vertical particle velocity at $t = 0.01$ ms. The snapshots correspond to the solid phase 1 (a), the solid phase 3 (b) and the fluid phase (c). The relative amplitude relation between the snapshots in Figures 2a), 2b) and 2c) is $1/157/3$, respectively.

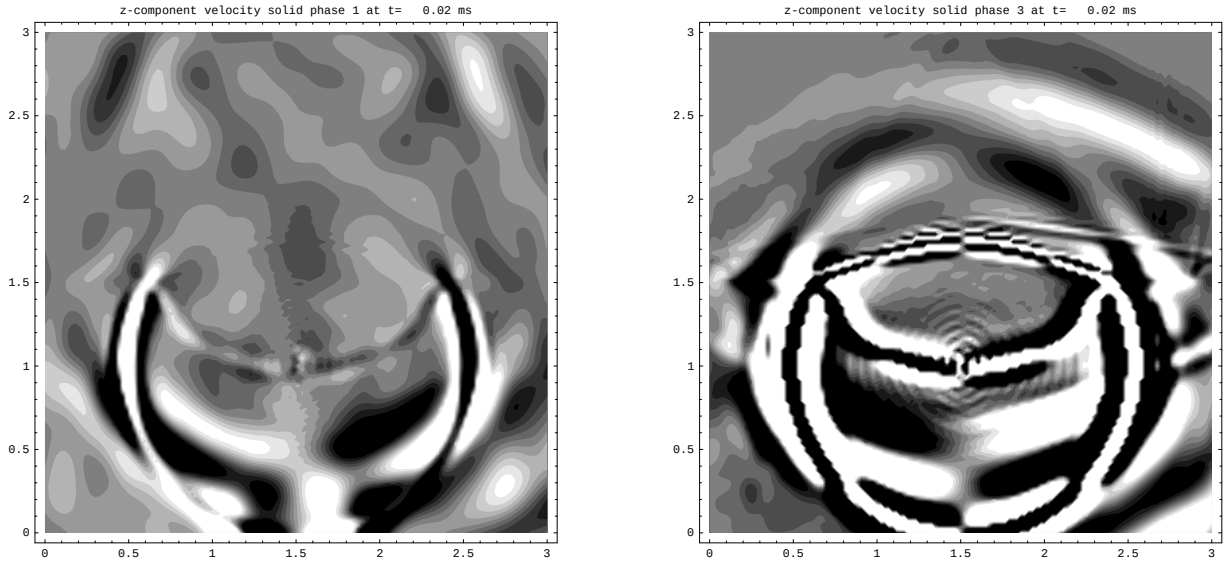

a) b)

Figure 3: Snapshots of the vertical particle velocity at $t = 0.01$ ms. The snapshots correspond to the solid phase 1 (a) and the solid phase 3 (b). The relative amplitude relation between the snapshots in Figures 2a) and 2b) and 2c) is $1/156$, respectively.

5 APPENDIX

5.1 The elastic coefficients

Let $K_{s1,m}, K_{s3,m},\ \mu_{s1,m}$ and $\mu_{s3,m}$ denote the bulk and shear modulus of the two solid (dry) frames, respectively. Also, let $K_{s1}, \mu_{s1}, K_{s3}, \mu_{s3}$ denote the bulk and shear moduli of the grains in the two solid phases, respectively, and let K_f denote the bulk modulus of the fluid phase. Then, following[5,7] the elastic coefficients are computed with the formulae:

$$\begin{aligned}
&\mu_j = [(1-g_j)\phi_1]^2\mu_{av} + \mu_{sj,m}, \quad g_j = \frac{\mu_{sj,m}}{\phi_1\mu_{sj}},\ j = 1,3,\\
&\mu_{13} = (1-g_1)(1-g_3)\phi_1\phi_3\mu_{av},\\
&\mu_{av} = \Big[\frac{(1-g_1)\phi_1}{\mu_{s1}} + \frac{\phi}{2\omega\eta} + \frac{(1-g_3)\phi_3}{\mu_{s3}}\Big]^{-1},\\
&K_{av} = \left[(1-c_1)\frac{\phi_1}{K_{s1}} + \frac{\phi}{K_f} + (1-c_3)\frac{\phi_3}{K_{s3}}\right]^{-1}, \quad c_j = \frac{K_{sj,m}}{\phi_1 K_{sj}},\ j = 1,3. \qquad (25)
\end{aligned}$$

For the remaining elastic coefficients, let

$$
\begin{aligned}
&K_{Gj} = K_{sj,m} + (\alpha_j)^2 K_{av}, \quad \alpha_j = S_j - \frac{K_{sj,m}}{K_{sj}},\\
&C_{12} = \phi K_{av}(\alpha_1 - S_1\phi),\\
&C_{23} = \phi K_{av}(\alpha_3 - S_3\phi),\\
&C_{13} = K_{av}(\alpha_1 - S_1\phi)(\alpha_3 - S_3\phi).
\end{aligned}
$$

The moduli K_{G1} and K_{G3} are the analogous of the Gassmann's moduli, while the coefficients α_1 and α_3 correspond to the effective stress coefficients in the classic Biot theory.[23,24] Then,

$$
\begin{aligned}
&\lambda_j = K_{Gj} - \frac{2}{3}\mu_j, \text{ (in 3D)}, \quad \lambda_j = K_{Gj} - \mu_j, \text{ (in 2D)} \quad , j = 1, 3,\\
&B_1 = \frac{S_1\phi^2 K_{av} + C_{12}}{\phi}, \quad B_2 = \frac{S_3\phi^2 K_{av} + C_{23}}{\phi},\\
&B_3 = \big(C_{13} + S_3 C_{12} + S_1 C_{23} + S_3 S_1 \phi^2 K_{av}\big).
\end{aligned}
$$

5.2 Modification of the Elastic Coefficients to Introduce Viscoelasticity

To introduce viscoelasticity we use the correspondence principle stated by M. Biot,[23,25] i.e. we replace the real poroelastic coefficients in the constitutive relations by complex frequency dependent poroviscoelastic moduli satisfying the same relations as in the elastic case. In this work we use the linear viscoelastic model presented in[26] to make the set of moduli $K_{G1}, K_{G3}, \mu_1, \mu_3, \mu_{1,3}$ and B_3 complex and frequency dependent, while all other coefficients in the constitutive relations remain real. The set of poroviscoelastic moduli is computed using the following formula:

$$
M(\omega) = \frac{M^*}{R_M(\omega) - iT_M(\omega)}, \tag{26}
$$

where the symbol 'M' represents the previously mentioned moduli and the coefficients M^* are reference values properly chosen to fit high frequency velocities usually measured in laboratory. The frequency dependent functions R_M and T_M, associated with a continuous spectrum of relaxation times, characterize the viscoelastic behaviour and are given by[26]

$$
R_M(\omega) = 1 - \frac{1}{\pi\widehat{Q}_M}\ln\frac{1+\omega^2 T_{1,M}^2}{1+\omega^2 T_{2,M}^2}, \qquad T_M(\omega) = \frac{2}{\pi\widehat{Q}_M}\tan^{-1}\frac{\omega(T_{1,M} - T_{2,M})}{1+\omega^2 T_{1,M}T_{2,M}}.
$$

The model parameters $\widehat{Q}_M$, $T_{1,M}$ and $T_{2,M}$ are taken such that the quality factors $Q_M(\omega) = T_M/R_M$ are approximately equal to $\widehat{Q}_M$ in the range of frequencies where the equations are solved, which makes this model convenient for geophysical applications.

5.3 Mass and Dissipative Coefficients

Let $\rho_m, m = 1, 2, 3$ denote the mass density of each solid and fluid constituent in Ω. Then, following[7,12] the frequency independent mass coefficients are computed by the relations

$$\begin{aligned}
m_{11} &= \rho_2\phi\left(1 + (S_1)^2 a_{32} + (S_3)^2 a_{12} - 2S_3 - (S_1)^2\right) + a_{13}\rho_1\phi_1 + (a_{31} - 1)\rho_3\phi_3,\\
m_{12} &= \rho_2\left(S_3(1 - a_{12}) + S_1 a_{32}\right),\\
m_{13} &= \rho_2\phi\left(1 - (S_1)^2 a_{32} - (S_3)^2 a_{12} - S_1 S_3\right) + \rho_1\phi_1(1 - a_{13}) + \rho_3\phi_3(1 - a_{31}),\\
m_{22} &= \frac{\rho_2}{\phi}\left(a_{12} + a_{32} - 1\right),\\
m_{23} &= \rho_2\left(S_1(1 - a_{32}) + S_3 a_{12}\right),\\
m_{33} &= \rho_2\phi\left(1 + (S_1)^2 a_{32} + (S_3)^2 a_{12} - 2S_1 - (S_3)^2\right) + a_{31}\rho_3\phi_3 + (a_{13} - 1)\rho_1\phi_1,
\end{aligned} \tag{27}$$

where

$$\begin{aligned}
a_{12} &= \frac{\phi_1\rho}{\phi\rho_2} r_{12} + 1, \quad a_{32} = \frac{\phi_3\rho'}{\phi\rho_2} r_{32} + 1,\\
a_{13} &= \frac{\phi_3\rho'}{\phi_1\rho_1} r_{13} + 1, \quad a_{31} = \frac{\phi_1\rho}{\phi_3\rho_3} r_{31} + 1.
\end{aligned}$$

The r_{ij}'s are the geometrical aspects of the boundaries separating the phases i and j (equal to $\frac{1}{2}$ for spheres) and

$$\rho = \frac{\phi\rho_2 + \phi_3\rho_3}{\phi + \phi_3}, \quad \rho' = \frac{\phi\rho_2 + \phi_1\rho_1}{\phi + \phi_1}.$$

Next, for the case of frozen porous media, following,[5] we define the dissipation coefficients d_{12}, d_{23} and d_{13} as follows:

$$\begin{aligned}
&d_{12} = (\phi)^2\frac{\eta}{\kappa_1}, \quad d_{23} = (\phi)^2\frac{\eta}{\kappa_3},\\
&d_{13} = \text{friction coefficient between the ice and the solid frames},
\end{aligned} \tag{28}$$

where η denotes the fluid viscosity and the permeability coefficients κ_1, κ_3 are defined in terms of the absolute permeabilities $\kappa_{1,0},\ \kappa_{3,0}$ of the two solid frames by the relations (see also[13])

$$\kappa_1 = \kappa_{1,0}\frac{(\phi)^3}{(1 - \phi_1)^3}, \quad \kappa_3 = \kappa_{3,0}\frac{(1 - \phi_1)^2}{\phi_3^2}\left(\frac{\phi}{\phi_1}\right)^3. \tag{29}$$

For the case of shaley sandstones, following[1] the coefficient d_{13} can be assumed to be zero and the friction coefficients d_{12} and d_{23} are taken to be of the form:

$$d_{12} = 45\eta R_{s1}^{-2}\phi^{-1}(1 - \phi)\phi_1, \ \ d_{23} = 45\eta R_{s3}^{-2}\phi^{-1}(1 - \phi)\phi_3, \tag{30}$$

where R_{s1}, R_{s3} denote the average radii of the sand and clay particles, respectively. The permeability coefficients are defined in this case by

$$\kappa_1 = 2\frac{R_{s1}^2}{9\phi_1} \quad \kappa_3 = 2\frac{R_{s3}^2}{9\phi_3}. \tag{31}$$

Next, the frequency independent friction coefficients for this model are given by

$$f_{11} = c_{11} + d_{13}, \qquad f_{12} = \frac{d_{12}S_3 - d_{23}S_1}{\phi}, \qquad f_{22} = \frac{d_{12} + d_{23}}{\phi^2}, \tag{32}$$

where $c_{11} = d_{12}S_3^2 + d_{23}S_1^2$.

In the high frequency range the set of inertial and friction coefficients are modified as follows. Let $F(\theta) = F_R(\theta) + iF_I(\theta)$, be the frequency correction function defined by Biot[27] in the high–frequency range:

$$F(\theta) = \frac{1}{4}\,\frac{\theta T(\theta)}{1 - \frac{2}{i\theta}T(\theta)}, \quad T(\theta) = \frac{\mathrm{ber}'(\theta) + i\mathrm{bei}'(\theta)}{\mathrm{ber}(\theta) + i\mathrm{bei}(\theta)},$$

with $\mathrm{ber}(\theta)$ and $\mathrm{bei}(\theta)$ being the Kelvin functions of the first kind and zero order. The frequency dependent argument $\theta = \theta(\omega)$ is given in terms of the pore size parameter a_p by the equations:

$$\theta = a_p\sqrt{\omega\,\rho_2/\eta}, \quad a_p = 2\sqrt{\kappa A_0/\phi}, \tag{33}$$

where $\dfrac{1}{\kappa} = \dfrac{1}{\kappa_1} + \dfrac{1}{\kappa_3}$ and A_0 is the Kozeny-Carman constant.[22,28] Then we define the frequency dependent mass and viscous coupling coefficients in the following fashion

$$\begin{aligned}
&p_{11}(\omega) = m_{11} + \frac{F_I(\theta)c_{11}}{\omega}, \quad p_{12}(\omega) = m_{12} - \frac{F_I(\theta)f_{12}}{\omega}, \\
&p_{13}(\omega) = m_{13} - \frac{F_I(\theta)c_{11}}{\omega}, \quad p_{22}(\omega) = m_{22} + \frac{F_I(\theta)f_{22}}{\omega}, \\
&p_{23}(\omega) = m_{23} + \eta\frac{F_I(\theta)f_{12}}{\omega}, \quad p_{33}(\omega) = p_{33} + \eta\frac{F_I(\theta)c_{11}}{\omega}
\end{aligned} \tag{34}$$

$$b_{11}(\omega) = \eta F_R(\theta)c_{11} + b_{13}, \quad b_{12}(\omega) = \eta F_R(\theta)f_{12}, \quad b_{22}(\omega) = \eta F_R(\theta)f_{22} \tag{35}$$

The coefficients d_{13} is left as a free parameter chosen so that the following condition is satisfied

$$b_{11}b_{22} - b_{12}^2 \geq 0. \tag{36}$$

6 CONCLUSIONS

A differential model describing wave propagation in a porous composite solid composed of two weakly-coupled phases saturated by a fluid is presented. The formulation is valid for the full frequency range since includes frequency dependent viscodynamic interaction among the two solids and the fluid.

The model is discretized using a finite element domain decomposition procedure and is applied for the numerical simulation of ultrasonic waves in a sample of water saturated partially frozen Berea sandstone.

The numerical experiment analyzes the response of the system in the presence of a plane horizontal interface defined by a change in ice content. The numerical results show that the model allows for an accurate description of the energy splitting at interfaces within the domain due to mode conversion from fast compressional and shear waves to slow waves and vice versa. The model also allows for the simulation of wave propagation in highly heterogeneous porous media such as fractal freezing or clay distribution in real hydrocarbon reservoir sandstones.

REFERENCES

[1] J. M. Carcione, B. Gurevich, and F. Cavallini. A generalized Biot-Gassmann model for the acoustic properties of shaley sandstones. *Geophysical Prospecting*, **48**, 539–557 (2000).

[2] J. L. Morack and J. C. Rogers. Seismic evidence of shallow permafrost beneath the islands in the Beafort Sea. *Arctic*, **3**, 166–174 (1981).

[3] J. M. Carcione and G. Seriani. Seismic velocities in permafrost. *Geophysical Prospecting*, **46**, 441–454 (1998).

[4] J. M. Carcione and G. Seriani. Wave simulation in frozen porous media. *J. Computational Physics*, **170**, 676–695 (2001).

[5] J. M. Carcione and U. Tinivella. Bottom-simulating reflectors: Seismic velocities and AVO effects. *Geophysics*, **65 (1)**, 54–67 (2000).

[6] S. Lee, P. Cornillon, and O. Campanella. Propagation of ultrasound waves through frozen foods. *Proceedings of the 2002 Annual Meeting and Food Expo., Anaheim (CA)*, (2002).

[7] J. E. Santos, C. L. Ravazzoli, and J. M. Carcione. A model for wave propagation in a composite solid matrix saturated by a single-phase fluid. *J. Acoust. Soc. Am.*, **115(6)**, 2749–2760 (2004).

[8] J. Douglas Jr, P. L. Paes Leme, J. E. Roberts, and J. Wang. A parallel iterative procedure applicable to the approximate solution of second order partial differential equations by mixed finite element methods. *Numer. Math.*, **65**, 95–108 (1993).

[9] J.Douglas Jr., J. E. Santos, D. Sheen, and X. Ye. Nonconforming Galerkin methods based on quadrilateral elements for second order elliptic problems. *RAIRO Math. Modeling and Numer. Analysis (M2AN)*, **33**, 747–770 (1999).

[10] P. A. Raviart and J. M. Thomas. Mixed finite element method for 2^{nd} order elliptic prob-

lems. *Mathematical Aspects of the Finite Element Methods, Lecture Notes of Mathematics, vol. 606, Springer*, (1975).

[11] J. C. Nedelec. Mixed finite elements in r^3. *Numer. Math.*, **35**, 315–341 (1980).

[12] J.M. Carcione, J. E. Santos, C. L. Ravazzoli, and H. B. Helle. Wave simulation in partially frozen porous media with fractal freezing conditions. *J. Appl. Physics*, **94**, 7839–7847 (2003).

[13] Ph. Leclaire, F. Cohen-Tenoudji, and J. Aguirre Puente. Extension of Biot's theory of wave propagation to frozen porous media. *J. Acoust. Soc. Amer.*, **96 (6)**, 3753–3767 (1994).

[14] Ph. Leclaire, F. Cohen-Tenoudji, and J. Aguirre Puente. Observation of two longitudinal and two transverse waves in a frozen porous medium. *J. Acoust. Soc. Amer.*, **97**, 2052–2055 (1995).

[15] D. Sheen. Finite element methods for an acoustic well-logging problem associated with a porous medium saturated by a two–phase immiscible fluid. *Numer. Methods for Partial Diff. Equations*, **9**, 155–174 (1993).

[16] J. Douglas Jr., J. E. Santos, and D. Sheen. Nonconforming galerkin methods for the helmholtz equation. *Numer. Methods for Partial Diff. Equations*, **17**, 475–494 (2001).

[17] T. Ha, J. E. Santos, and D. Sheen. Nonconforming finite element methods for the simulation of waves in viscoelastic solids. *Computer Methods in Appl. Mech. and Eng.*, **191**, 5647–5670 (2002).

[18] F. I. Zyserman, P. M. Gauzellino, and J. E. Santos. Dispersion analysis of a nonconforming finite element method for the helmholtz and elastodynamic equations. *Int. J. Numer. Meth. Eng.*, **58**, 1381–1395 (2003).

[19] J. Douglas Jr., J. E. Santos, D. Sheen, and L. Bennethum. Frequency domain treatment of one–dimensional scalar waves. *Math. Models Methods Appl. Sci.*, **3**, 171–194 (1993).

[20] J. E. Santos, C. L Ravazzoli, P. M. Gauzellino, J. M. Carcione, and F. Cavallini. Simulation of waves in poro-viscoelastic rocks saturated by inmiscible fluids. numerical evidence of a second slow wave. *Journal of Computational Acoustics*, **12(1)**, 1–21 (2004).

[21] G. T. Kuster and M. N. Toksöz. Velocity and attenuation of seismic waves in two-phase media: Part 1. Theoretical formulations. *Geophysics*, **39**, 587–606 (1974).

[22] J. M. Hovem and G. D. Ingram. Viscous attenuation of sound in saturated sand. *J. Acoust. Soc. Amer.*, **66**, 1807–1812 (1979).

[23] M. A. Biot. Mechanics of deformation and acoustic propagation in porous media. *J. Appl. Phys.*, **33**, 1482–1498 (1962).

[24] J. M. Carcione. Wave fields in real media: Wave propagation in anisotropic, anelastic and porous media. *Handbook of Geophysical Exploration,Pergamon Press Inc.*, **31** (2001).

[25] M. A. Biot. Theory of deformation of a porous viscoelastic anisotropic solid. *J. Appl. Phys.*, **27**, 459–467 (1956).

[26] H. P. Liu, D. L. Anderson, and H. Kanamori. Velocity dispersion due to anelasticity; implications for seismology and mantle composition. *Geophys. J. R. Astr. Soc.*, **l47**, 41–

58 (1976).
[27] M. A. Biot. Theory of propagation of elastic waves in a fluid-saturated porous solid. II. High frequency range. *J. Acoust. Soc. Am.*, **28**, 179–191 (1956).
[28] J. Bear. Dynamics of fluids in porous media. *Dover Publications, New York*, (1972).
[29] M. A. Biot. Theory of propagation of elastic waves in a fluid-saturated porous solid. I. Low frequency range. *J. Acoust. Soc. Am.*, **28**, 168–171 (1956).